Parallel Implementation of High-Fidelity Multiqubit Gates with Neutral Atoms

Harry Levine[1,*] Alexander Keesling[1] Giulia Semeghini[1] Ahmed Omran[1] Tout T. Wang[1,2] Sepehr Ebadi,[1]
Hannes Bernien,[3] Markus Greiner,[1] Vladan Vuletić,[4] Hannes Pichler,[1,5] and Mikhail D. Lukin[1]

[1]*Department of Physics, Harvard University, Cambridge, Massachusetts 02138, USA*
[2]*Department of Physics, Gordon College, Wenham, Massachusetts 01984, USA*
[3]*Pritzker School of Molecular Engineering, University of Chicago, Chicago, Illinois 60637, USA*
[4]*Department of Physics and Research Laboratory of Electronics, Massachusetts Institute of Technology,
Cambridge, Massachusetts 02139, USA*
[5]*ITAMP, Harvard-Smithsonian Center for Astrophysics, Cambridge, Massachusetts 02138, USA*

We report the implementation of universal two- and three-qubit entangling gates on neutral-atom qubits encoded in long-lived hyperfine ground states. The gates are mediated by excitation to strongly interacting Rydberg states and are implemented in parallel on several clusters of atoms in a one-dimensional array of optical tweezers. Specifically, we realize the controlled-phase gate, enacted by a novel, fast protocol involving only global coupling of two qubits to Rydberg states. We benchmark this operation by preparing Bell states with fidelity $\mathcal{F} \geq 95.0(2)\%$, and extract gate fidelity $\geq 97.4(3)\%$, averaged across five atom pairs. In addition, we report a proof-of-principle implementation of the three-qubit Toffoli gate, in which two control atoms simultaneously constrain the behavior of one target atom. These experiments demonstrate key ingredients for high-fidelity quantum information processing in a scalable neutral-atom platform.

Trapped neutral atoms are attractive building blocks for large scale quantum information systems. They can be readily manipulated in large numbers while maintaining excellent quantum coherence, as has been demonstrated in remarkable quantum simulation and precision measurement experiments [1,2]. Single atom initialization, addressing, and readout have been demonstrated in a variety of optical trapping platforms, and single-qubit gates have been implemented with exquisite fidelity [3–5]. Multiqubit entangling gates with neutral atoms can be implemented by driving atoms to highly excited Rydberg states, which exhibit strong and long-range interactions [6]. Protocols for entangling atoms using Rydberg interactions have been explored theoretically and experimentally over the last decade [7–13], but despite major advances, progress in this field has been limited by relatively low fidelities associated with ground-state–Rydberg-state coherent control [14]. Recent advances in Rydberg atom control [15–17] offer new opportunities for realization of entangling gates, combining high-fidelity performance and parallelization.

In this Letter, we introduce a new method for realizing multiqubit entangling gates between individual neutral atoms trapped in optical tweezers. In our approach, qubits are encoded in long-lived hyperfine states $|0\rangle$ and $|1\rangle$ which can be coherently manipulated individually or globally to perform single-qubit gates. Our two-qubit gate, the controlled-phase gate, is implemented with a novel protocol consisting of just two global laser pulses which drive nearby atoms within the Rydberg blockade regime [7].

We benchmark this gate by preparing Bell states of two atoms with a fidelity $\mathcal{F} \geq 95.0(2)\%$, averaged across five pairs of atoms. After accounting for state preparation and measurement (SPAM) errors, we extract the entanglement operation fidelity to be $\mathcal{F}^c \geq 97.4(3)\%$, competitive with other leading platforms capable of simultaneous manipulation of ten or more qubits [18–21]. Additionally, we demonstrate a proof-of-principle implementation of the three-qubit Toffoli gate, wherein two atoms simultaneously constrain a third atom through the Rydberg blockade, highlighting the potential use of Rydberg interactions for efficient multiqubit operations [14,22].

In our experiments, individual ^{87}Rb atoms are trapped in optical tweezers and sorted by a real-time feedback procedure into groups of two or three, organized in a one-dimensional array [23–25]. We encode qubits in the hyperfine ground states of these atoms, with $|0\rangle = |5S_{1/2}, F = 1, m_F = 0\rangle$ and $|1\rangle = |5S_{1/2}, F = 2, m_F = 0\rangle$. In each experiment, we initialize all qubits in $|0\rangle$ through a Raman-assisted optical pumping procedure [26]. Single-qubit coherent control is achieved through a combination of a global laser field which homogeneously drives all qubits, as well as local addressing lasers which apply ac Stark shifts on individual qubits [Figs. 1(a) and 1(b)]. The global drive field is generated by a 795 nm laser, tuned near the $5S_{1/2}$ to $5P_{1/2}$ transition. This laser is intensity modulated to produce sidebands which drive the qubits through a two-photon Raman transition with an effective Rabi frequency $\Omega_{01} \approx 2\pi \times 250$ kHz [Fig. 1(e)] [26,27]. The local
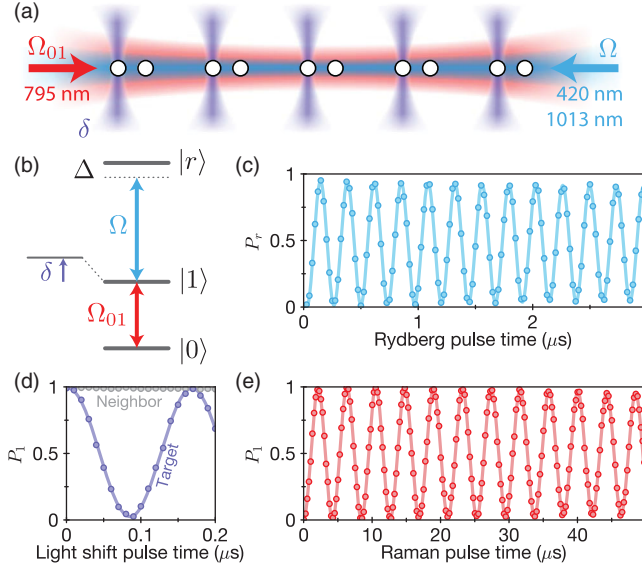
FIG. 1. Control of individual qubits in atom arrays. (a) Atoms arranged in pairs are globally driven with a 795 nm Raman laser (shown in red) which couples the hyperfine qubit levels. Local 420 nm beams (purple) are focused onto individual sites, resulting in a light shift δ used for individual addressing. Additionally, atoms are globally excited by a bichromatic Rydberg laser (shown in blue) containing 420 nm and 1013 nm light from the $|1\rangle$ qubit state to $|r\rangle$. (b) Relevant atomic levels. The qubit states are $|0\rangle = |5S_{1/2}, F = 1, m_F = 0\rangle$ and $|1\rangle = |5S_{1/2}, F = 2, m_F = 0\rangle$. The qubit state $|1\rangle$ is coupled to the Rydberg state $|r\rangle = |70S_{1/2}, m_J = -1/2\rangle$ with detuning Δ and Rydberg Rabi frequency Ω. (c) Rydberg Rabi oscillations from $|1\rangle$ to $|r\rangle$. Only one atom in each pair is prepared in state $|1\rangle$ to avoid interactions. Atoms in $|r\rangle$ are directly detected by loss from tweezers [17]. (d) Local phase shifts as measured in a Ramsey sequence, averaged across the five atom pairs. The purple curve belongs to the addressed atom and shows high-contrast oscillations; the gray curve shows the nonaddressed atom, which sees limited $<2\%$ crosstalk. (e) Rabi oscillations from $|0\rangle$ to $|1\rangle$ driven by Raman lasers. Error bars in all figures denote 68% confidence intervals and, in most cases, are smaller than the markers.

addressing beams are generated by an acousto-optic deflector which splits a single 420 nm laser, tuned near the $5S_{1/2}$ to $6P_{3/2}$ transition, into several beams focused onto individual atoms [Figs. 1(a) and 1(d)] [17]. We describe these two couplings as global $X(\theta)$ qubit rotations and local $Z(\theta)$ rotations. After each sequence, we measure the individual qubit states by pushing atoms in $|1\rangle$ out of the traps with a resonant laser pulse, followed by a site-resolved fluorescence image of the remaining atoms [26].

We perform multiqubit gates by exciting atoms from the qubit state $|1\rangle$ to the Rydberg state $|r\rangle = |70S_{1/2}, m_J = -1/2\rangle$. All atoms are homogeneously coupled from $|1\rangle$ to $|r\rangle$ through a two-photon process with effective Rabi frequency $\Omega \approx 2\pi \times 3.5$ MHz [Fig. 1(c)] [26]. Within a given cluster of atoms, the Rydberg interaction between nearest neighbors is

$2\pi \times 24$ MHz $\gg \Omega$; neighboring atoms, therefore, evolve according to the Rydberg blockade in which they cannot be simultaneously excited to the Rydberg state [7].

To entangle atoms in such arrays, we introduce a new protocol for the two-qubit controlled-phase (CZ) gate that relies only on global excitation of atoms within the Rydberg blockade regime. The desired unitary CZ gate maps the computational basis states as follows:

$$
\begin{aligned}
|00\rangle &\rightarrow |00\rangle, \\
|01\rangle &\rightarrow |01\rangle e^{i\phi}, \\
|10\rangle &\rightarrow |10\rangle e^{i\phi}, \\
|11\rangle &\rightarrow |11\rangle e^{i(2\phi-\pi)}.
\end{aligned}
\tag{1}
$$

This map is equivalent to the canonical form of the controlled-phase gate $\mathcal{CZ} = 2|00\rangle\langle00| - \mathbb{1}$ up to a single-qubit phase ϕ. To realize this gate, we use two global Rydberg laser pulses of the same length τ and detuning Δ which couple $|1\rangle$ to $|r\rangle$, with the laser phase of the second pulse shifted by ξ (Fig. 2).

The gate can be understood by considering the behavior of the four computational basis states. The $|00\rangle$ state is uncoupled by the laser field and, therefore, does not evolve. The dynamics of $|01\rangle$ (and $|10\rangle$) are given by the coupling of the single atom on the $|1\rangle \leftrightarrow |r\rangle$ transition, forming a two-level system with Rabi frequency Ω and detuning Δ [Fig. 2(c), top]. The $|11\rangle$ state evolves within the Rydberg blockade regime as a two-level system due to the collective coupling from $|11\rangle \leftrightarrow |W\rangle = (1/\sqrt{2})(|1r\rangle + |r1\rangle)$, with enhanced Rabi frequency $\sqrt{2}\Omega$ and the same detuning Δ [Fig. 2(c), bottom]. For a chosen detuning Δ, we select the pulse length τ such that the first laser pulse completes a full cycle of a detuned Rabi oscillation for the $|11\rangle$ system. The same pulse drives an incomplete Rabi oscillation on the $|01\rangle$ system. A subsequent phase jump $\Omega \rightarrow \Omega e^{i\xi}$ rotates the orientation of the drive field around the Z axis by an angle ξ such that a second pulse of length τ completes the oscillation and returns the state to $|01\rangle$, while driving a second complete detuned oscillation on the $|11\rangle$ configuration. By the end of the second pulse, both $|01\rangle$ and $|11\rangle$ return to their initial positions on the Bloch sphere but with accumulated dynamical phases ϕ_{01} and ϕ_{11}, which depend on the geometric surface area of the Bloch sphere enclosed by the Δ-dependent trajectories. As shown in Fig. 2(d), for a specific choice of laser detuning ($\Delta \approx 0.377\,\Omega$), $2\phi_{01} - \pi = \phi_{11}$, realizing the CZ gate (1). Remarkably, this gate protocol is faster (total time $2\tau \approx 2.732\pi/\Omega$) than the traditional approach [7] of sequential local pulses (total time $4\pi/\Omega$), and offers the additional advantage of requiring only global coupling of both qubits.

We demonstrate the parallel operation of the CZ gate on five separate pairs of atoms by using it to create Bell states of the form $|\Phi^+\rangle = (1/\sqrt{2})(|00\rangle + |11\rangle)$. We initialize all
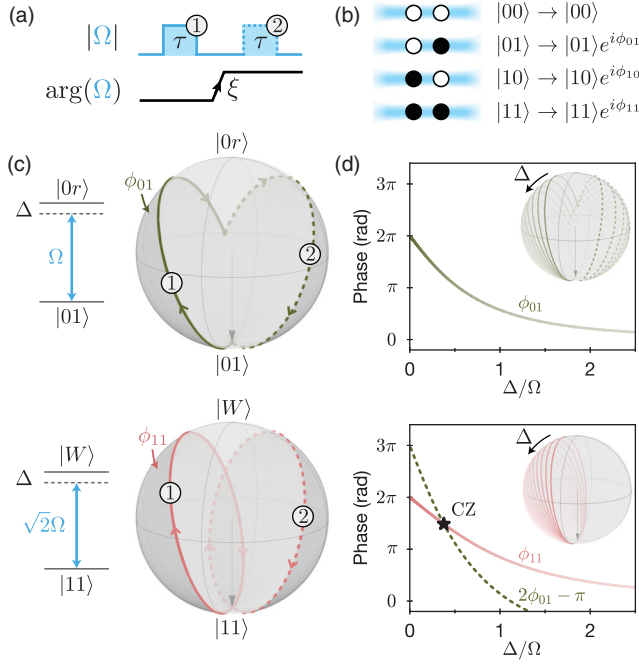
FIG. 2. Controlled-phase (CZ) gate protocol. (a) Two global Rydberg pulses of length τ and detuning Δ drive Bloch sphere rotations around two different axes due to a laser phase change ξ between pulses. (b) As a result of the evolution, each basis state returns to itself with an accumulated dynamical phase. $|00\rangle$ is uncoupled and, therefore, accumulates no phase. $|01\rangle$ and $|10\rangle$ are equivalent by symmetry ($\phi_{01} = \phi_{10}$), while $|11\rangle$ accumulates phase ϕ_{11}. The CZ gate is realized for $\phi_{11} = 2\phi_{01} - \pi$. (c) The dynamics of the $|01\rangle$ and $|11\rangle$ states can be understood in terms of two-level systems with the same detuning Δ but different effective Rabi frequencies. The pulse length τ is chosen such that the $|11\rangle$ system undergoes a complete detuned Rabi cycle during the first pulse, while the $|01\rangle$ system undergoes an incomplete oscillation. The laser phase ξ is chosen such that the second pulse drives around a different axis to close the trajectory for the $|01\rangle$ system, while driving a second complete cycle for the $|11\rangle$ system. (d) The dynamical phases ϕ_{01} and ϕ_{11} are determined by the shaded area enclosed by the Bloch sphere trajectory and vary from 2π to 0 as a function of Δ, corresponding to increasingly shallow trajectories. Insets show family of trajectories for different detunings. Choosing $\Delta \approx 0.377\,\Omega$ realizes the CZ gate.

atomic qubits in $|0\rangle$, then apply a global $X(\pi/2)$ Raman pulse to prepare each atom in $|-\rangle_y = (1/\sqrt{2})(|0\rangle - i|1\rangle)$. The CZ gate protocol, consisting of the two Rydberg laser pulses, is then applied over a total time of 0.4 μs, during which the optical tweezers are turned off to avoid antitrapping of the Rydberg state. The pulse sequence realizes map (1), along with an additional phase rotation on each qubit due to the light shift of the Rydberg lasers on the hyperfine qubit states. We embed the CZ gate implementation in an echo sequence to cancel the effect of the light shift, and we add an additional short light shift to eliminate the single-particle phase ϕ [26]. Altogether, this realizes a unitary that
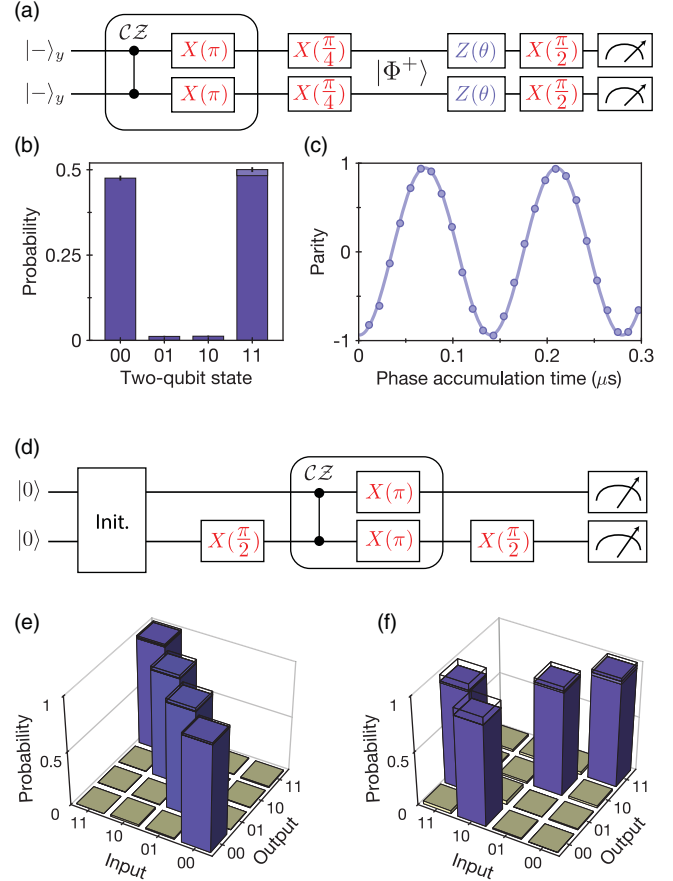

FIG. 3. Bell state preparation and controlled-NOT (CNOT) gate. (a) Quantum circuit used to prepare and probe the $|\Phi^+\rangle$ state. (b) Measured populations of the Bell states. Raw measurements associating $|0\rangle$ with atom presence and $|1\rangle$ with atom absence yields 97.6(2)% in the target states. Separate measurements of leakage out of the qubit subspace indicate a small contribution (light shaded region) to these probabilities; subtracting this contribution, the measured population is $\geq 95.8(3)\%$. (c) The parity oscillation with respect to accumulated phase θ has a measured amplitude of 94.2(4)%. The resulting lower bound on Bell state fidelity is $\mathcal{F} \geq 95.0(2)\%$ [raw measurements yield $\mathcal{F}^{\mathrm{raw}} = 95.9(2)\%$]. Correction for SPAM errors results in $\mathcal{F}^{\mathrm{c}} \geq 97.4(3)\%$. (d) The CNOT gate is constructed from our native CZ gate with the addition of local hyperfine qubit rotations. (e) The four computational basis states are prepared with average fidelity 96.8(2)%. (f) We apply the CNOT sequence to the four computational basis states and measure the truth table fidelity to be $\mathcal{F}_{\mathrm{CNOT}} \geq 94.1(2)\%$. Corrected for SPAM errors, the fidelity is $\mathcal{F}^{\mathrm{c}}_{\mathrm{CNOT}} \geq 96.5(3)\%$. Wire frames on purple bars show ideal outcomes; solid bars show the raw measurement; the light-shaded top portions of the bars bound the contribution from qubit leakage. Only the darker lower region is counted towards fidelities.

combines the canonical CZ gate with a global $X(\pi)$ gate [enclosed region in Figs. 3(a) and 3(d)]. A final $X(\pi/4)$ rotation produces the Bell state $|\Phi^+\rangle$ [Fig. 3(a)] [26].

We characterize the experimentally produced state ρ by evaluating its fidelity with respect to the target Bell state $\mathcal{F} = \langle\Phi^+|\rho|\Phi^+\rangle$. The fidelity is the sum of two terms, the

first of which is the Bell state populations, given by the probability of observing $|00\rangle$ or $|11\rangle$ [Fig. 3(b)]. The second term is the coherence between $|00\rangle$ and $|11\rangle$, measured by applying a global $Z(\theta)$ rotation followed by a global $X(\pi/2)$ rotation and observing parity oscillations [Figs. 3(a) and 3(c)] [28]. When evaluating the contributions to the fidelity, we account for atom population left in the Rydberg state after the operation and for background losses. Both of these correspond to leakage out of the qubit subspace and can lead to overestimation of the $|1\rangle$ populations and Bell state fidelities in the raw measurements. Using separate measurements of atoms in both hyperfine qubit states [26], we determine a conservative upper bound on these leakage errors and subtract this contribution (shown in light shaded regions of bar plots in Figs. 3 and 4, see [26]). The resulting lower bound on the Bell state fidelity is $\mathcal{F} \geq 95.0(2)\%$.

The measured Bell state fidelity includes errors in state preparation and measurement, as well as errors in the two-qubit entangling gate. To characterize the entangling gate specifically, we evaluate the error contributions from SPAM (1.2(1)% per atom) and compute a SPAM-corrected fidelity $\mathcal{F}^c \geq 97.4(3)\%$ [26]. The majority of the remaining error is due to finite atomic temperature and laser scattering during Rydberg dynamics [26]. We separately characterize our native $\mathcal{CZ}$ gate by converting it to a controlled-NOT (CNOT) gate via local rotations [Fig. 3(d)]. We measure the action of the CNOT gate on each computational basis state to obtain its truth table fidelity $\mathcal{F}^c_{\text{CNOT}} \geq 96.5(3)\%$, corrected for SPAM errors (Figs. 3(e) and 3(f)] [26].

Finally, we extend our control of multiple atomic qubits to implement the three-qubit controlled-controlled-phase (CCZ) gate. This logic operation can be decomposed into five two-qubit gates [29–31]. Instead, we realize this multiple-control gate directly by preparing three atoms in the nearest-neighbor blockade regime such that both outer atoms constrain the behavior of the middle atom. The complicated three-atom dynamics makes it challenging to analytically construct global laser pulses that realize a CCZ gate in this configuration. Therefore, we use numerical optimization to construct a global amplitude and frequency modulated laser pulse which approximately implements the CCZ gate [26]. The laser pulse is optimized through the remote dressed chopped random basis (RedCRAB) optimal control algorithm [32,33].

We implement the CCZ gate in parallel on four triplets of atomic qubits [Fig. 4(a)]. The three atoms in each triplet are arranged such that nearest neighbors are blockaded by the strong $2\pi \times 24$ MHz interaction, as in the two-qubit experiments. The edge atoms interact with each other weakly ($2\pi \times 0.4$ MHz). As with the two-qubit gate, we embed the CCZ gate in an echo sequence to cancel light shifts, such that our gate implements CCZ along with a global $X(\pi)$ rotation. To characterize the performance of this three-qubit gate, we convert it into a Toffoli gate by applying a local
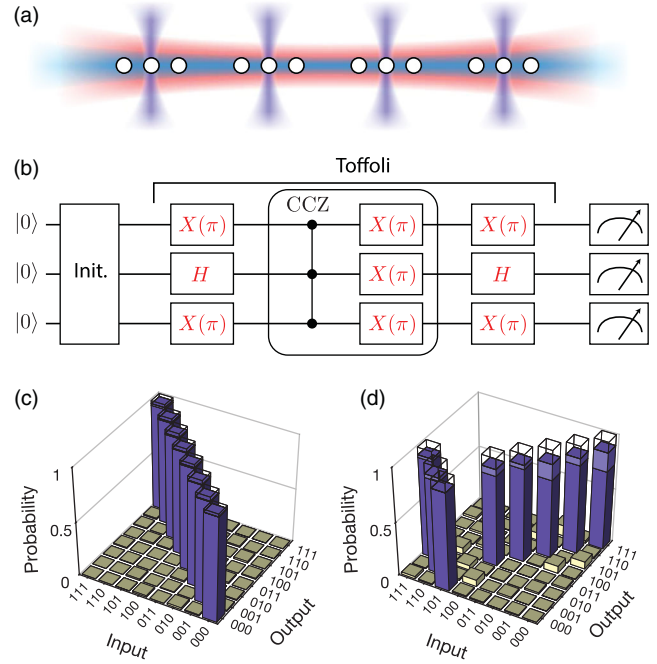

FIG. 4. Realization of three-qubit Toffoli gate. (a) The Toffoli gate is implemented in parallel on four triplets of atomic qubits using the same lasers as for two-qubit gates. (b) Quantum circuit for constructing the Toffoli gate from local rotations and a globally implemented CCZ gate. (c) Eight computational basis states are prepared with average fidelity 95.3(3)%. (d) Measured truth table, with fidelity $\mathcal{F}_{\text{Toff}} \geq 83.7(3)\%$. Corrected for SPAM errors, the fidelity is $\mathcal{F}^c_{\text{Toff}} \geq 87.0(4)\%$. Wire frames on purple bars show ideal outcomes; solid bars show the raw measurement; the light-shaded top portions of the bars bound the contribution from qubit leakage. Only the darker lower region is counted towards fidelities.

Hadamard on the middle atom before and after the CCZ gate [along with edge $X(\pi)$ pulses, to simplify implementation [26]] [Fig. 4(b)]. We apply the Toffoli gate to each computational basis state to measure the truth table fidelity $\mathcal{F}^c_{\text{Toff}} \geq 87.0(4)\%$, corrected for SPAM errors [Figs. 4(c) and 4(d)] [26]. Additionally, we perform "limited tomography," consisting of truth table measurements in a rotated basis, to verify the phases of the Toffoli unitary in a more experimentally accessible manner than full process tomography [31]. The limited tomography (LT) fidelity is $\mathcal{F}^c_{\text{LT}} \geq 86.2(6)\%$ [26].

These results can be directly improved and extended along several directions. The fidelity of Rydberg coupling is primarily limited by finite atomic temperature and off-resonant laser scattering, which can be addressed by sideband cooling of atoms within optical tweezers [34,35] and by higher power lasers. The background atomic loss and state preparation can be improved using higher quality vacuum systems [36] and more sophisticated state preparation techniques [5]. Finally, atomic qubit readout can be improved using recently demonstrated nondestructive

readout protocols [5,37,38] to give stronger constraints on the atomic populations.

While, in this Letter, we have performed parallel gate implementation on spatially separated clusters of atoms, the same approach can be extended to nonlocal coupling within contiguous atom arrays using local addressing with an additional off-resonant laser system. Specifically, subsets of the array could be simultaneously illuminated to create light shifts that bring them into resonance with a global resonant Rydberg excitation laser [26]. Furthermore, with more atoms arranged in the blockade volume, the controlled-phase gate demonstrated here can be extended to higher multiqubit gates with global coupling [26]. The dipolar interaction between S and P Rydberg states [39] could also be used to achieve improved gate connectivity between qubits. A combination of the present results with recently demonstrated trapping and rearrangement of individual neutral atoms in 2D and 3D [24,40,41] will be well-suited for the implementation of deep quantum circuits or variational quantum optimization with hundreds of qubits [42]. In addition, such a platform could be utilized to explore efficient methods for error correction and fault-tolerant operation to eventually enable scalable quantum processing.

M. G., V. V., and M. D. L. have an equity interest in and serve on the advisory board of QuEra Computing.

Note added.—Recently, we became aware of related work demonstrating neutral-atom gates in two-dimensional atom arrays [43].

---

*Corresponding author.
hlevine@g.harvard.edu

[1] C. Gross and I. Bloch, Quantum simulations with ultracold atoms in optical lattices, Science **357**, 995 (2017).

[2] X. Zhang and J. Ye, Precision measurement and frequency metrology with ultracold atoms, Natl. Sci. Rev. **3**, 189 (2016).

[3] T. Xia, M. Lichtman, K. Maller, A. W. Carr, M. J. Piotrowicz, L. Isenhower, and M. Saffman, Randomized Benchmarking of Single-Qubit Gates in a 2D Array of Neutral-Atom Qubits, Phys. Rev. Lett. **114**, 100503 (2015).

[4] Y. Wang, A. Kumar, T.-Y. Wu, and D. S. Weiss, Single-qubit gates based on targeted phase shifts in a 3d neutral atom array, Science **352**, 1562 (2016).

[5] T.-Y. Wu, A. Kumar, F. Giraldo, and D. S. Weiss, Stern-Gerlach detection of neutral-atom qubits in a state-dependent optical lattice, Nat. Phys. **15**, 538 (2019).

[6] A. Browaeys, D. Barredo, and T. Lahaye, Experimental investigations of dipole-dipole interactions between a few Rydberg atoms, J. Phys. B **49**, 152001 (2016).

[7] D. Jaksch, J. I. Cirac, P. Zoller, S. L. Rolston, R. Côté, and M. D. Lukin, Fast Quantum Gates for Neutral Atoms, Phys. Rev. Lett. **85**, 2208 (2000).

[8] M. Saffman, T. G. Walker, and K. Mølmer, Quantum information with Rydberg atoms, Rev. Mod. Phys. **82**, 2313 (2010).

[9] T. Wilk, A. Gaëtan, C. Evellin, J. Wolters, Y. Miroshnychenko, P. Grangier, and A. Browaeys, Entanglement of Two Individual Neutral Atoms Using Rydberg Blockade, Phys. Rev. Lett. **104**, 010502 (2010).

[10] L. Isenhower, E. Urban, X. L. Zhang, A. T. Gill, T. Henage, T. A. Johnson, T. G. Walker, and M. Saffman, Demonstration of a Neutral Atom Controlled-NOT Quantum Gate, Phys. Rev. Lett. **104**, 010503 (2010).

[11] Y.-Y. Jau, A. M. Hankin, T. Keating, I. H. Deutsch, and G. W. Biedermann, Entangling atomic spins with a Rydberg-dressed spin-flip blockade, Nat. Phys. **12**, 71 (2016).

[12] Y. Zeng, P. Xu, X. He, Y. Liu, M. Liu, J. Wang, D. J. Papoular, G. V. Shlyapnikov, and M. Zhan, Entangling Two Individual Atoms of Different Isotopes via Rydberg Blockade, Phys. Rev. Lett. **119**, 160502 (2017).

[13] C. J. Picken, R. Legaie, K. McDonnell, and J. D. Pritchard, Entanglement of neutral-atom qubits with long ground-Rydberg coherence times, Quantum Science and Technology **4**, 1 (2018).

[14] M. Saffman, Quantum computing with atomic qubits and Rydberg interactions: Progress and challenges, J. Phys. B **49**, 202001 (2016).

[15] S. de Léséleuc, D. Barredo, V. Lienhard, A. Browaeys, and T. Lahaye, Analysis of imperfections in the coherent optical excitation of single atoms to Rydberg states, Phys. Rev. A **97**, 053803 (2018).

[16] H. Levine, A. Keesling, A. Omran, H. Bernien, S. Schwartz, A. S. Zibrov, M. Endres, M. Greiner, V. Vuletić, and M. D. Lukin, High-Fidelity Control and Entanglement of Rydberg-Atom Qubits, Phys. Rev. Lett. **121**, 123603 (2018).

[17] A. Omran, H. Levine, A. Keesling, G. Semeghini, T. T. Wang, S. Ebadi, H. Bernien, A. S. Zibrov, H. Pichler, S. Choi, J. Cui, M. Rossignolo, P. Rembold, S. Montangero, T. Calarco, M. Endres, M. Greiner, V. Vuletić, and M. D. Lukin, Generation and manipulation of Schrödinger cat states in Rydberg atom arrays, Science **365**, 570 (2019).

[18] K. Wright et al., Benchmarking an 11-qubit quantum computer, arXiv:1903.08181.

[19] A. Erhard, J. J. Wallman, L. Postler, M. Meth, R. Stricker, E. A. Martinez, P. Schindler, T. Monz, J. Emerson, and R. Blatt, Characterizing large-scale quantum computers via cycle benchmarking, arXiv:1902.08543.

[20] M. Gong *et al.*, Genuine 12-Qubit Entanglement on a Superconducting Quantum Processor, Phys. Rev. Lett. **122**, 110501 (2019).

[21] K. X. Wei, I. Lauer, S. Srinivasan, N. Sundaresan, D. T. McClure, D. Toyli, D. C. McKay, J. M. Gambetta, and S. Sheldon, Verifying multipartite entangled GHZ states via multiple quantum coherences, arXiv:1905.05720.

[22] H. Weimer, M. Müller, I. Lesanovsky, P. Zoller, and H. P. Büchler, A Rydberg quantum simulator, Nat. Phys. **6**, 382 (2010).

[23] M. Endres, H. Bernien, A. Keesling, H. Levine, E. R. Anschuetz, A. Krajenbrink, C. Senko, V. Vuletić, M. Greiner, and M. D. Lukin, Atom-by-atom assembly of defect-free one-dimensional cold atom arrays, Science **354**, 1024 (2016).

[24] D. Barredo, S. de Léséleuc, V. Lienhard, T. Lahaye, and A. Browaeys, An atom-by-atom assembler of defect-free arbitrary 2D atomic arrays, Science **354**, 1021 (2016).

[25] H. Kim, W. Lee, H. Lee, H. Jo, Y. Song, and J. Ahn, *In situ* single-atom array synthesis using dynamic holographic optical tweezers, Nat. Commun. **7**, 13317 (2016).

[26] See Supplemental Material at http://link.aps.org/supplemental/10.1103/PhysRevLett.123.170503 for additional technical details and measurements pertaining to the main text.

[27] D. D. Yavuz, P. B. Kulatunga, E. Urban, T. A. Johnson, N. Proite, T. Henage, T. G. Walker, and M. Saffman, Fast Ground State Manipulation of Neutral Atoms in Microscopic Optical Traps, Phys. Rev. Lett. **96**, 063001 (2006).

[28] C. A. Sackett, D. Kielpinski, B. E. King, C. Langer, V. Meyer, C. J. Myatt, M. Rowe, Q. A. Turchette, W. M. Itano, D. J. Wineland, and C. Monroe, Experimental entanglement of four particles, Nature (London) **404**, 256 (2000).

[29] A. Barenco, C. H. Bennett, R. Cleve, D. P. DiVincenzo, N. Margolus, P. Shor, T. Sleator, J. A. Smolin, and H. Weinfurter, Elementary gates for quantum computation, Phys. Rev. A **52**, 3457 (1995).

[30] A. Fedorov, L. Steffen, M. Baur, M. P. da Silva, and A. Wallraff, Implementation of a Toffoli gate with superconducting circuits, Nature (London) **481**, 170 (2012).

[31] C. Figgatt, D. Maslov, K. A. Landsman, N. M. Linke, S. Debnath, and C. Monroe, Complete 3-qubit Grover search on a programmable quantum computer, Nat. Commun. **8**, 1918 (2017).

[32] N. Rach, M. M. Müller, T. Calarco, and S. Montangero, Dressing the chopped-random-basis optimization: A bandwidth-limited access to the trap-free landscape, Phys. Rev. A **92**, 062343 (2015).

[33] R. Heck *et al.*, Remote optimization of an ultracold atoms experiment by experts and citizen scientists, Proc. Natl. Acad. Sci. U.S.A. **115**, E11231 (2018).

[34] A. M. Kaufman, B. J. Lester, and C. A. Regal, Cooling a Single Atom in an Optical Tweezer to its Quantum Ground State, Phys. Rev. X **2**, 041014 (2012).

[35] J. D. Thompson, T. G. Tiecke, A. S. Zibrov, V. Vuletić, and M. D. Lukin, Coherence and Raman Sideband Cooling of a Single Atom in an Optical Tweezer, Phys. Rev. Lett. **110**, 133001 (2013).

[36] J. P. Covey, I. S. Madjarov, A. Cooper, and M. Endres, 2000-Times Repeated Imaging of Strontium Atoms in Clock-Magic Tweezer Arrays, Phys. Rev. Lett. **122**, 173201 (2019).

[37] M. Martinez-Dorantes, W. Alt, J. Gallego, S. Ghosh, L. Ratschbacher, Y. Völzke, and D. Meschede, Fast Nondestructive Parallel Readout of Neutral Atom Registers in Optical Potentials, Phys. Rev. Lett. **119**, 180503 (2017).

[38] M. Kwon, M. F. Ebert, T. G. Walker, and M. Saffman, Parallel Low-Loss Measurement of Multiple Atomic Qubits, Phys. Rev. Lett. **119**, 180504 (2017).

[39] S. de Léséleuc, D. Barredo, V. Lienhard, A. Browaeys, and T. Lahaye, Optical Control of the Resonant Dipole-Dipole Interaction between Rydberg Atoms, Phys. Rev. Lett. **119**, 053202 (2017).

[40] D. Barredo, V. Lienhard, S. de Léséleuc, T. Lahaye, and A. Browaeys, Synthetic three-dimensional atomic structures assembled atom by atom, Nature (London) **561**, 79 (2018).

[41] A. Kumar, T.-Y. Wu, F. Giraldo, and D. S. Weiss, Sorting ultracold atoms in a three-dimensional optical lattice in a realization of Maxwell's demon, Nature (London) **561**, 83 (2018).

[42] H. Pichler, S.-T. Wang, L. Zhou, S. Choi, and M. D. Lukin, Quantum optimization for maximum independent set using Rydberg atom arrays, arXiv:1808.10816.

[43] T. M. Graham, M. Kwon, B. Grinkemeyer, Z. Marra, X. Jiang, M. T. Lichtman, Y. Sun, M. Ebert, and M. Saffman, Rydberg mediated entanglement in a two-dimensional neutral atom qubit array, arXiv:1908.06103.